RSC Advances

PAPER

Cite this: *RSC Adv.*, 2023, **13**, 17449

A palladium(0)–threonine complex immobilized on the surface of magnetic mesocellular foam: an efficient, stable, and magnetically separable nanocatalyst for Suzuki, Stille, and Heck cross-coupling reactions†

Zeinab Shirvandi,[a] Arash Ghorbani-Choghamarani *[b] and Amin Rostami*[a]

Received 24th April 2023
Accepted 29th May 2023

DOI: 10.1039/d3ra02721j

rsc.li/rsc-advances

In this study, a new palladium nanocatalyst was supported on L-threonine functionalized magnetic mesocellular silica foams (MMCF@Thr-Pd) and was characterized by FT-IR, XRD, BET, SEM, EDS, VSM, TGA, ICP-OES and elemental mapping techniques. The obtained MMCF@Thr-Pd performance can show excellent catalytic activity for Stille, Suzuki, and Heck coupling reactions, and the corresponding products were obtained with high yields. More importantly, the efficient and stable MMCF@Thr-Pd nanocatalyst was recovered by applying an external magnetic field and reused for at least five consecutive runs without a change in the catalytic activity.

Introduction

The carbon–carbon bond formation reaction is one of the basic and necessary reactions in organic synthesis, the pharmaceutical industry, and in current research.[1,2] These reactions exist in the procurement of natural products, polymers, drugs, and pharmaceuticals compounds, herbicides, and industrially important materials.[3–5] It is well known that Suzuki, Stille, and Heck reactions are efficient techniques for C–C bond formation owing to their good tolerance to different functional groups.[6,7] Among the noble metals, palladium-based complexes are the most beneficial catalysts for carbon–carbon cross-coupling in organic transformations. The application of cross-coupling reactions depends on the activity and stability of the palladium complexes.[8–10] The most representative palladium catalysts are palladium salts or homogenous complexes coordinated with various phosphine ligands, providing excellent catalytic activity.[11–13] However, nothing is perfect, and this kind of homogeneous catalysis suffers from serious drawbacks, which limit their applications to a certain extent.[14,15] The most important inconvenience found in homogeneous catalyst deals with the fact that the catalyst cannot be easily separated from the reaction mixture and reused.[16–18] This also means that the desired isolated products are usually contaminated with heavy metal, which irremediably leads to negative environmental effects and increases the total cost of catalyzed synthesis.[19,20] Additionally, commonly used palladium complexes and catalysts are expensive and not easily recyclable. To solve these issues, the heterogenization of homogeneous catalysts, especially heavy metal complexes, and expensive palladium nanoparticles on the surface of the organic and inorganic solid hosts, has been developed.[21–23] Different supports such as metal oxides[24] zeolites[25] carbon materials[26] and mesoporous silica[27] are used for the immobilization of palladium nanoparticles. Among various supporters, magnetic nanoparticles have attracted great attention due to their inherent magnetic properties, low toxicity, easy synthesis, environmental-friendly, easy separation, and reusability in consecutive reactions.[28,29] However, magnetic nanoparticles suffer from limited participation of available active sites, severe catalyst leaching, poor long-time dispersibility, and stability, which may reason new difficulties including low catalytic activity and selectivity.[30,31] This defect can be minimized by using mesocellular silica foam (MCF), a mesoporous material consisting of spherical cells and windows. Their structure has large spherical cell pores (20–42 nm) interconnected with small cylindrical window pores (8–22 nm) to form a continuous three-dimensional (3D) porous structure.[32,33] Because MCF silica nanostructure has a high surface area (500–1000 $m^2 g^{-1}$), large pore size, and large pore volume, a large number of active sites can be created on the inner walls of mesocellular foam channels by surface modification. Thus, MCF silica material is an appropriate candidate for use as support for catalysts, as drug delivery carriers, and as the stationary phase in chromatography.[34] However, the

[a]Department of Chemistry, Faculty of Science, University of Kurdistan, 66177-15175, Sanandaj, Iran. E-mail: a.rostami@uok.ac.ir

[b]Department of Organic Chemistry, Faculty of Chemistry, Bu-Ali Sina University, 6517838683 Hamedan, Iran. E-mail: a.ghorbani@basu.ac.ir; arashghch58@yahoo.com

† Electronic supplementary information (ESI) available. See DOI: https://doi.org/10.1039/d3ra02721j

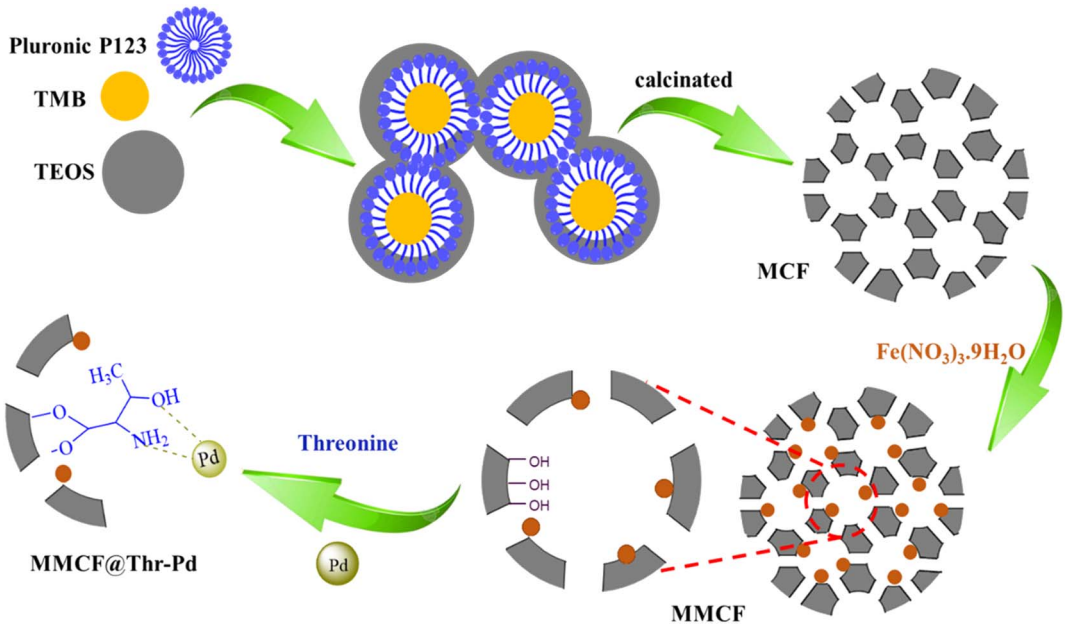

Scheme 1 Synthesis of MMCF@Thr-Pd

problems in separation and pollution of the products by small particles of residual mesoporous silica catalysts severely limit their applications economically, catalytic, and industrial processes. Consequently, researchers have sought alternative catalytic systems that offer similar activity and selectivity, but are easier to separate and reuse.[35,36] Thus, mesoporous magnetic nanocomposite has emerged as a family of new functional nanoparticles in recent years. Mesoporous magnetic nanocomposite has attracted wide attention owing to the combination of the prominent properties of mesoporous materials (high surface area and large pore size) and properties of magnetic nanoparticles (magnetic separation capability) in drug-targeted delivery, bioseparation, and new-generated catalysts.[37,38]

L-Threonine (Thr) is an essential amino acid produced by yeasts on an industrial scale and has an extensive range of commercial applications, such as a food additive and agricultural feed supplement. Its structure consists of a carboxyl group, an α-amino group, and a side chain containing a hydroxyl group, which makes it a polar and uncharged amino acid. The N–H group of L-threonine, which may form a hydrogen bond with the O–H groups on a mesoporous magnetic surface, can help accelerate the immobilization process by being beside the carboxylic acid group.[39] Also, functional groups on its side chains remain available to coordinate metal ions and form the final complex. For this reason, the amino acid L-threonine was used as a green, inexpensive, and efficient promoter for the synthesis of palladium catalysts.

In the present work, γ-Fe_2O_3 magnetic nanoparticles were encapsulated using the convenient synthesis methodology into mesoporous channels of the MCF silica materials to form mesoporous magnetic nanocomposite and were used as the

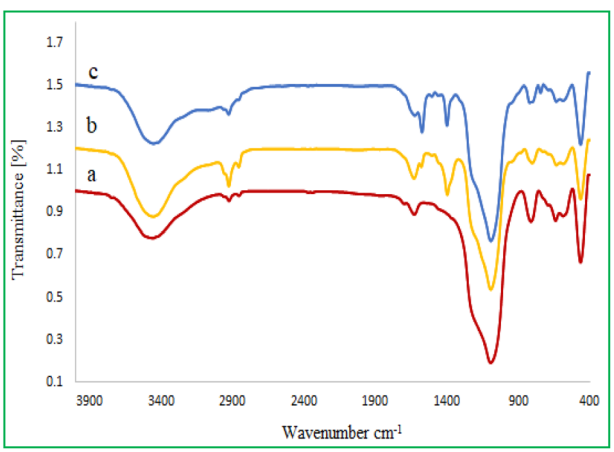

Fig. 1 FT-IR spectra of (a) MMCF, (b) MMCF@Thr, and (c) MMCF@Thr-Pd.

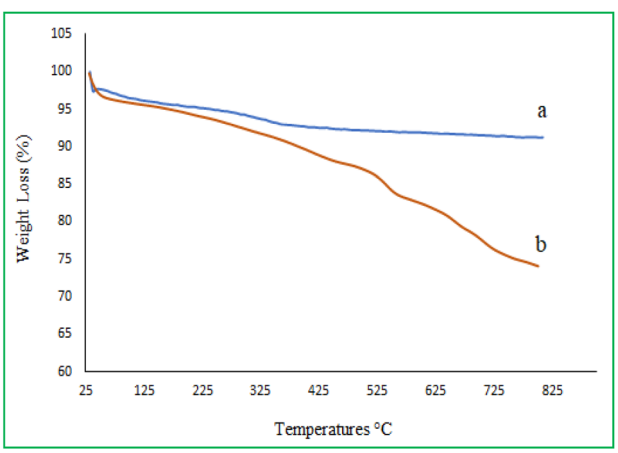

Fig. 2 TGA curves of (a) MMCF, (b) MMCF@Thr-Pd.

support to prepare palladium nanocatalyst (MMCF@Thr-Pd) (Scheme 1). Then MMCF@Thr-Pd was identified using different analytical techniques and its catalytic activity was studied as an effective, green, and recyclable nanocatalyst for carbon–carbon bond formation through Suzuki, Stille, and Heck reactions under mild and phosphine-free conditions.

Result and discussion

Catalyst characterizations

Fig. 1 displays the FT-IR spectrum of (a) MMCF, (b) M-MCF@Thr, and (c) MMCF@Thr-Pd. In all figures, the symmetric and asymmetric vibrations of Si–O–Si bonds at 468, 808, and 1087 cm^{-1} and the stretching vibration of Fe–O bonds at 584 and 638 cm^{-1} reveal the embedding of MNP nanoparticles into MCF. Also, the absorption band around 3460 cm^{-1} corresponds to the O–H stretching vibrations and is visible in all spectra. In Fig. 1b, two prominent bands at 2858 and 2927 cm^{-1} are observed, which are assigned to the aliphatic C–H stretching of amino acid L-threonine. The presence of absorption bands at 1396 cm^{-1} can correspond to C–N stretching vibrations, 1692 cm^{-1} and 1575 cm^{-1} are associated with the C=O and N–H vibrations, which confirm the successful attachment of the amino acid L-threonine on the surface of MMCF. In the case of Fig. 1c, we noted that the N–H stretching vibration bands of $-NH_2$ shifted to a lower wave number (1575 cm^{-1} to 1550 cm^{-1}). The above is indicated that the bonding interactions are formed between the functional groups of the amino acid L-threonine with palladium nanoparticles.

Thermal stability of (a) MMCF and (b) MMCF@ThrPd was determined using TGA analysis. As shown in Fig. 2a, the MMCF shows a 2.3% weight loss at around 200 °C due to the evaporation of physically adsorbed moisture. Also, between 200 and 500 °C, M-MCF loses about 3.5% of its weight due to the condensation process between the surface Si–OH groups. The thermogram of the MMCF@Thr-Pd shows two stages of weight loss (Fig. 2b). The weight loss (2%) below 200 °C may be due to the removal of moisture and organic solvent present on the surface of the MMCF@Thr-Pd nanocatalyst. The other weight loss (8.2%) between 200 and 655 °C may be due to the breakdown of L-threonine bonds and the degradation of the complex Pd coated on the surface of M-MCF nanoparticles. Thus, the

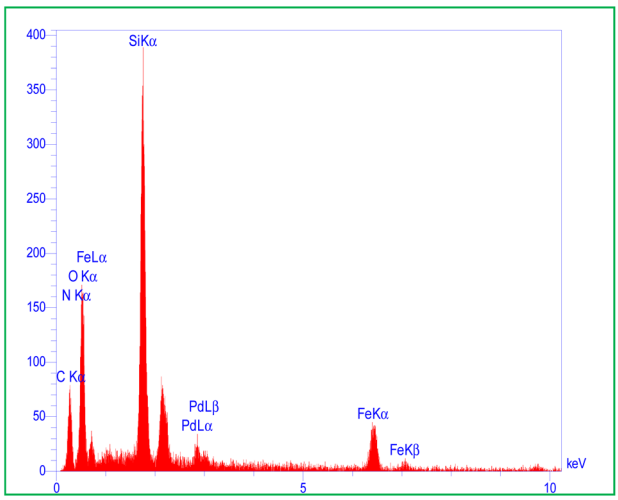

Fig. 3 EDS spectrum of MMCF@Thr-Pd.

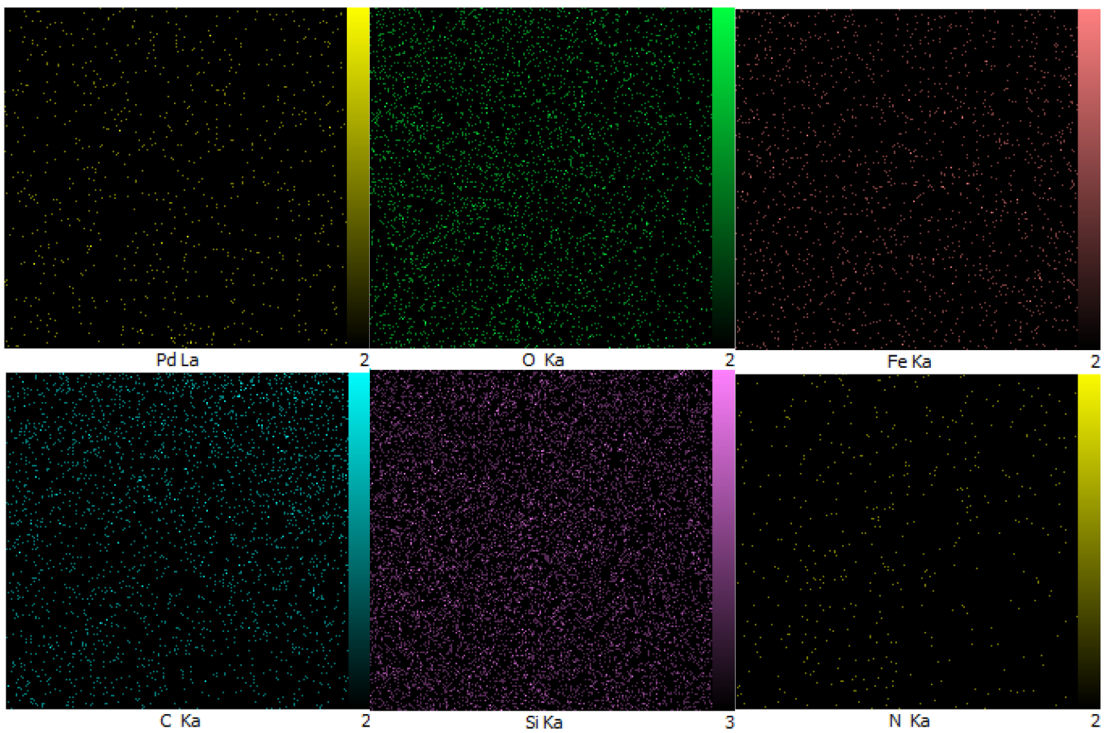

Fig. 4 Elemental mapping of MMCF@Thr-Pd.

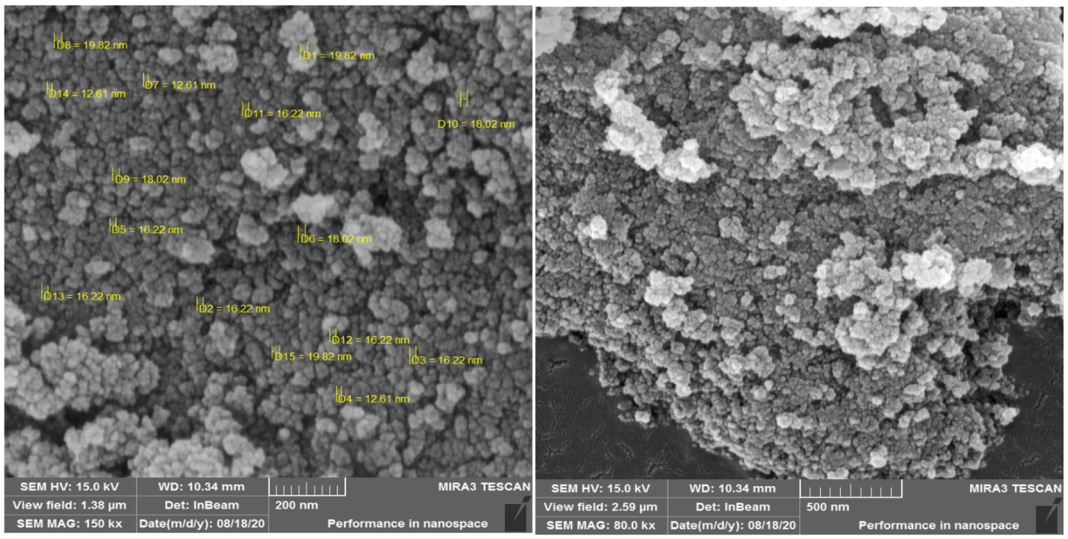

Fig. 5 SEM images of MMCF@Thr-Pd.

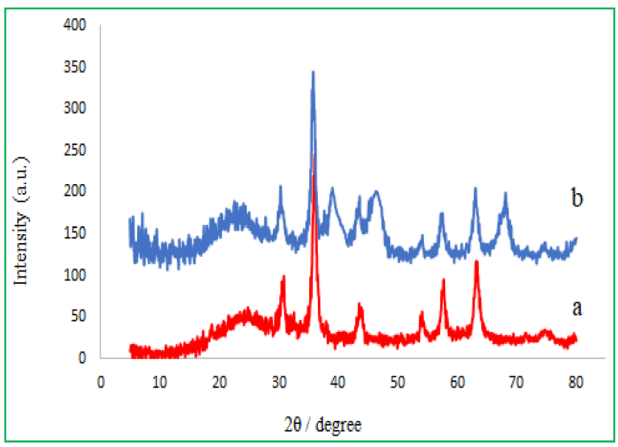

Fig. 6 XRD patterns of (a) MMCF, (b) MMCF@Thr-Pd.

above results show that the MMCF@Thr-Pd nanocatalyst has high thermal stability and is suitable for use in most organic reactions.

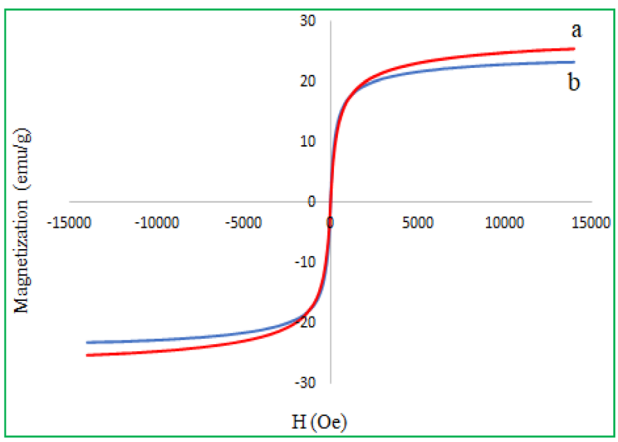

Fig. 7 Magnetization curves for (a) MMCF, (b) MMCF@Thr-Pd.

The elemental compositions of MMCF@Thr-Pd were determined by energy-dispersive X-ray (EDS) spectrum (Fig. 3) and their distributions were confirmed by the EDS mappings (Fig. 4). As shown in Fig. 3, the EDS analysis of MMCF@Thr-Pd nanoparticles verified the presence of Fe, C, Si, O, N, and Pd elements. Additionally, a homogeneous distribution of the elements was indicated by EDS mapping of MMCF@Thr-Pd (Fig. 4). Additionally, the amount of palladium loading on MMCF nanoparticles was determined by ICP-OES, which was found to be 1.59 mmol g^{-1}.

The structure of the MMCF@Thr-Pd nanocatalyst was surveyed by scanning electron microscopy (SEM). SEM image of the MMCF@Thr-Pd nanocatalyst is presented in Fig. 5. As shown in the SEM images, the M-MCF@Thr-Pd nanoparticles have a uniform quasi-spherical morphology with diameters of about 15–25 nm.

The high-angle XRD patterns of the M-MCF particles and MMCF@Thr-Pd nanocatalyst were recorded, and their diagrams are shown in Fig. 6. A broad peak in the range of 16–28 degrees was detected in both samples, which were assigned to amorphous silica. In addition, both samples show six diffraction peaks identical with 2θ = 30.3°, 35.8°, 43.4°, 53.8°, 57.3° and 63.0°, which correspond to the crystalline phase of γ-Fe_2O_3. This result means that the magnetic nanoparticles have been successfully placed within the MCF pore.[40] In the XRD spectrum of MMCF@Thr-Pd nanocatalyst (Fig. 6b), the presence of all peaks related to γ-Fe_2O_3 nanoparticles confirmed that the coating of the palladium complex did not change the phase of γ-Fe_2O_3 nanoparticles. Also, three new peaks at 2θ = 40.1°, 46.6°, and 68.0° corresponding to Pd crystal plates were observed in the MMCF@Thr-Pd nanocatalyst spectrum,[41] indicating that the Pd(0) complex was successfully immobilized on the surface of MMCF nanoparticles.

The magnetic measurements of the MMCF and MMCF@Thr-Pd were examined by a vibrating sample magnetometer (VSM) at room temperature in an applied magnetic field of up to 60 000 Oe, and the magnetization curves are shown in Fig. 7. These samples show superparamagnetic behavior and have

Table 1 Textural properties of MMCF and nanocatalyst MMCF@Thr-Pd

Sample	BET surface area ($m^2\ g^{-1}$)	Pore diameter by BJH method (nm)		Pore volume ($cm^3\ g^{-1}$)
		Window (nm)	Cell (nm)	
M-MCF	285.95	15.01	25.85	1.01
MMCF@Thr-Pd	168.89	14.40	22.61	0.57

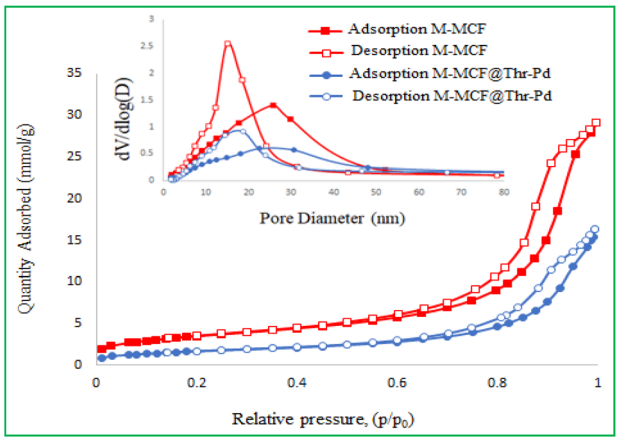

Fig. 8 Nitrogen adsorption–desorption isotherms of (a) MMCF, (b) MMCF@Thr-Pd.

a saturation magnetization of 25.44 emu g^{-1} and 23.26 emu g^{-1}, respectively. As can be seen, the saturation magnetization values in the MMCF@Thr-Pd nanocatalyst are reduced compared to the M-MCF nanoparticles. This is due to the loading of L-threonine and Pd nanoparticles on the surface of the M-MCF support.

The textural properties of the MMCF@Thr-Pd nanocatalyst studied using N_2 adsorption/desorption analysis are reported in Table 1 and compared to a pure M-MCF. The N_2 adsorption–desorption isotherms are shown in Fig. 8. As observed, the isotherms exhibit a type IV behavior, with a hysteresis loop, that is characteristic of mesoporous materials.[42] The surface area, pore volume, window size, and cell size of M-MCF were 285.95 $m^2\ g^{-1}$, 1.01 $cm^3\ g^{-1}$, 15.01, and 25.85 nm, respectively. After the modification of MMCF with Pd complexes, the amount of N_2 adsorbed decreased significantly, and accordingly, the surface area, pore volume, window size, and cell size changed to 168.89 $m^2\ g^{-1}$, 0.57 $cm^3\ g^{-1}$, 14.40, and 22.61 nm, respectively. These results confirm a fine coating of the Pd complex inside the magnetic mesocellular foams.

Catalytic studies

The catalytic property of the MMCF@Thr-Pd nanocatalyst was initially examined in the Suzuki cross-coupling reaction. The

Table 2 Optimization of the reaction conditions for the coupling reaction of iodobenzene with phenylboronic acid in the presence of M-MCF@Thr-Pd[a]

Entry	Catalyst (mmol)	Solvent	Base (3 mmol)	Temp. (°C)	Time (min)	Yield[b] (%)
1	—	EtOH	K_2CO_3	60	10 h	N.R
2	0.0079	EtOH	K_2CO_3	60	20	95
3	0.0079	DMF	K_2CO_3	60	20	48
4	0.0079	PEG200	K_2CO_3	60	20	88
5	0.0079	DMSO	K_2CO_3	60	20	40
6	0.0079	H_2O	K_2CO_3	60	20	70
7	0.0079	Dioxane	K_2CO_3	60	20	38
8	0.0079	EtOH	KOH	60	20	88
9	0.0079	EtOH	NaOH	60	20	72
10	0.0079	EtOH	Et_3N	60	20	45
11	0.0079	EtOH	Na_2CO_3	60	20	78
12	0.0047	EtOH	K_2CO_3	60	20	80
13	0.0111	EtOH	K_2CO_3	60	20	96
14	0.0079	EtOH	K_2CO_3	80	20	96
15	0.0079	EtOH	K_2CO_3	40	20	58
16[c]	0.0079	EtOH	K_2CO_3	60	20	60
17[d]	0.0079	EtOH	K_2CO_3	60	20	45

[a] Reaction conditions: iodobenzene (1 mmol), phenylboronic acid (1 mmol), base (3 mmol), catalyst and solvent (2 mL). [b] Isolated yield. [c] Complex Thr-Pd as the catalyst. [d] MMCF@Pd as the catalyst.

Table 3 Catalytic Suzuki coupling reaction of aryl halides with phenylboronic acid in the presence of MMCF@Thr-Pd

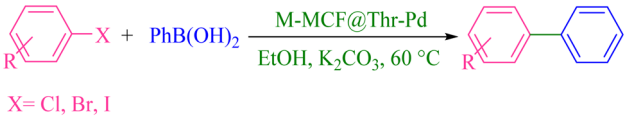

Entry	Ar–X	Product	Time (min)	Yield[a,b] (%)	TOF (h^{-1})
1	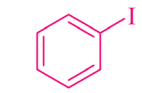	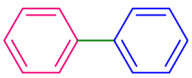	20	95	360.75
2	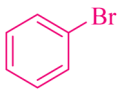	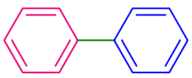	35	91	197.46
3	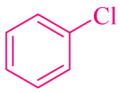	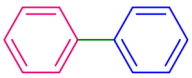	180	86	36.28
4	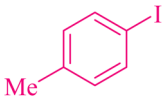	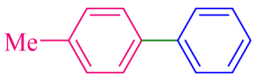	45	93	156.96
5	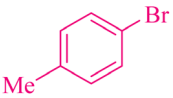	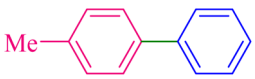	80	93	88.29
6	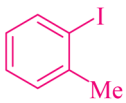	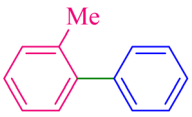	50	91	138.22
7	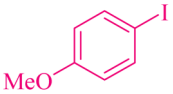	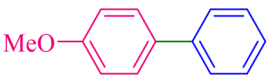	35	95	206.14
8	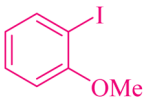		50	92	139.74
9	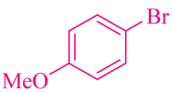	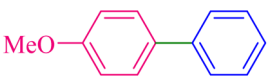	50	90	136.70
10	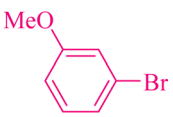	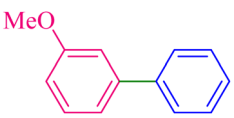	70	93	100.90
11	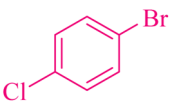	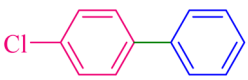	80	92	87.34
12	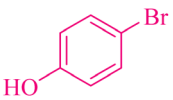	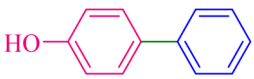	35	96	208.31
13	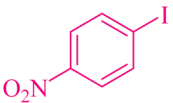	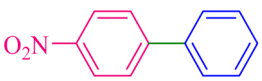	90	92	77.63

Table 3 (*Contd.*)

Entry	Ar–X	Product	Time (min)	Yield[a,b] (%)	TOF (h^{-1})
14	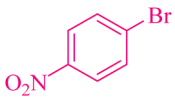	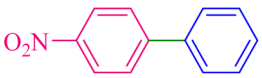	100	88	66.83
15	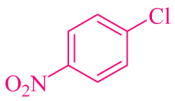	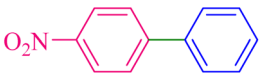	180	75	31.64

[a] Reaction conditions: aryl halides (1 mmol), phenylboronic acid (1 mmol), K_2CO_3 (3 mmol), M-MCF@Thr-Pd (0.0079 mmol), EtOH (2 mL) and 60 °C. [b] Isolated yield.

Table 4 Optimization of the reaction conditions for the coupling reaction of iodobenzene with triphenyltin chloride in the presence of MMCF@Thr-Pd[a]

Entry	Catalyst (mmol)	Solvent	Base (3 mmol)	Temp. (°C)	Time (min)	Yield[b] (%)
1	—	PEG200	K_2CO_3	80	10 h	N.R
2	0.0111	PEG200	K_2CO_3	80	40	95
3	0.0079	PEG200	K_2CO_3	80	40	95
4	0.0047	PEG200	K_2CO_3	80	40	86
5	0.0079	DMF	K_2CO_3	80	40	65
6	0.0079	EtOH	K_2CO_3	80	40	78
7	0.0079	DMSO	K_2CO_3	80	40	70
8	0.0079	H_2O	K_2CO_3	80	40	68
9	0.0079	Dioxane	K_2CO_3	80	40	20
10	0.0079	PEG200	KOH	80	40	70
11	0.0079	PEG200	NaOH	80	40	64
12	0.0079	PEG200	Et_3N	80	40	55
13	0.0079	PEG200	Na_2CO_3	80	40	85
14	0.0079	PEG200	K_2CO_3	100	40	96
15	0.0079	PEG200	K_2CO_3	60	40	56

[a] Reaction conditions: iodobenzene (1 mmol), triphenyltin chloride (0.5 mmol), base (3 mmol), catalyst and solvent (2 mL). [b] Isolated yield.

reaction of iodobenzene with phenylboronic acid in the presence of MMCF@Thr-Pd nanocatalyst was selected as the model reaction for optimization of different reaction conditions including base, solvent types, amount of catalyst, and temperature. As shown in Table 2, the model reaction was first tested using different solvents, among which EtOH was more appropriate for the Suzuki cross-coupling reaction and gave the highest yield (Table 2, entries 2–7). Then, different bases such as NaOH, KOH, Et_3N, K_2CO_3, and Na_2CO_3 were screened for their effect on the reaction (Table 2, entries 8–11); it was found that K_2CO_3 with the yield is 95% more effective. Next, the effect of the catalyst amount was examined. With increasing the amount of catalyst, the yield of the desired product does not increase, but by decreasing the amount of MMCF@Thr-Pd nanocatalyst (Table 2, entries 9–13), the yield of the desired product decreases. Finally, the effect of different temperatures was investigated, and the results showed that 60 °C was more appropriate than other temperatures (Table 2, entries 14, 15).

Table 5 Catalytic Stille coupling reaction of aryl halides with triphenyltin chloride in the presence of MMCF@Thr-Pd

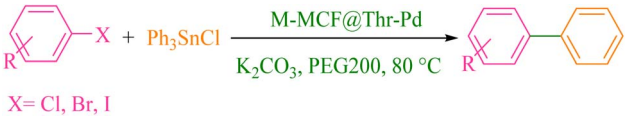

Entry	Ar–X	Product	Time (min)	Yield[a,b] (%)	TOF (h^{-1})
1	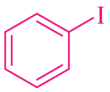	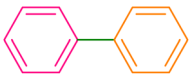	40	95	180.37
2	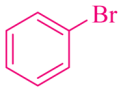		120	90	56.96
3	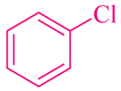		240	76	24.05
4	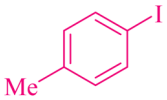	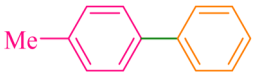	60	92	116.45
5	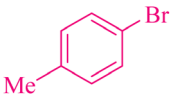	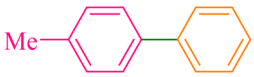	80	88	83.54
6	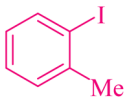	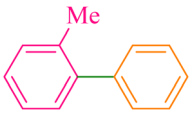	90	90	75.94
7	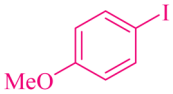	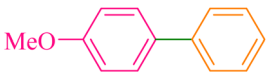	35	90	195.29
8	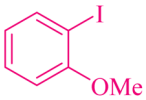	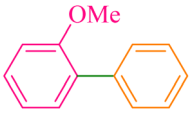	55	89	122.89
9	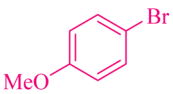	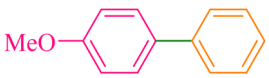	70	88	95.47
9	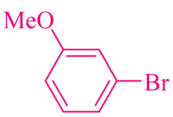	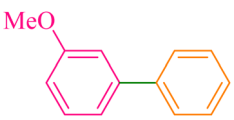	90	85	71.72
11	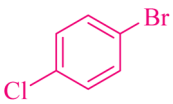	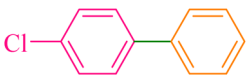	130	88	51.41
12	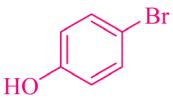	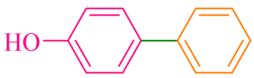	65	90	105.16
13	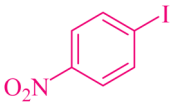	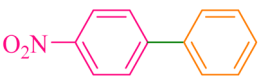	120	90	56.96

Table 5 (*Contd.*)

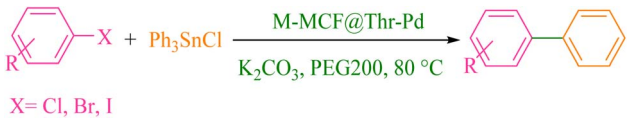

Entry	Ar–X	Product	Time (min)	Yield[a,b] (%)	TOF (h^{-1})
14	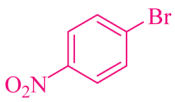	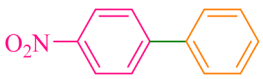	150	88	44.55
15	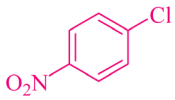	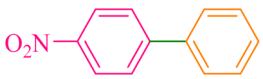	240	70	22.15

[a] Reaction conditions: aryl halides (1 mmol), triphenyltin chloride (0.5 mmol), K_2CO_3 (3 mmol), M-MCF@Thr-Pd (0.0079 mmol), PEG200 (2 mL) and 80 °C. [b] Isolated yield.

Table 6 Optimization of the reaction conditions for the coupling reaction of iodobenzene with *n*-butyl acrylate in the presence of MMCF@Thr-Pd[a]

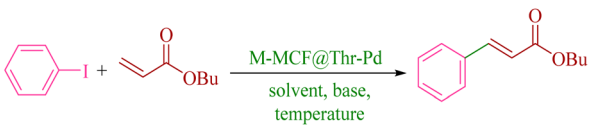

Entry	Catalyst (mmol)	Solvent	Base (3 mmol)	Temp. (°C)	Time (min)	Yield[b] (%)
1	—	PEG200	Na_2CO_3	100	10 h	N.R
2	0.0159	PEG200	Na_2CO_3	100	30	96
3	0.0127	PEG200	Na_2CO_3	100	30	96
4	0.0079	PEG200	Na_2CO_3	100	30	78
5	0.0047	PEG200	Na_2CO_3	100	30	54
6	0.0127	DMF	Na_2CO_3	100	30	93
7	0.0127	DMSO	Na_2CO_3	100	30	80
8	0.0127	Dioxane	Na_2CO_3	100	30	30
9	0.0127	PEG200	KOH	80	30	55
10	0.0127	PEG200	NaOH	80	30	60
11	0.0127	PEG200	Et_3N	80	30	74
12	0.0127	PEG200	K_2CO_3	80	30	88
13	0.0127	PEG200	Na_2CO_3	80	30	65
14	0.0127	PEG200	Na_2CO_3	60	30	97

[a] Reaction conditions: iodobenzene (1 mmol), *n*-butyl acrylate (1.2 mmol), base (3 mmol), catalyst and solvent (2 mL). [b] Isolated yield.

Next, we evaluated the Suzuki coupling reaction of iodobenzene with phenylboronic acid in the presence of the unsupported palladium complex (L-threonine ligand with Pd(0) ions: Thr-Pd) under optimized conditions (Table 2, entry 2). When the model reaction was carried out under homogeneous conditions, the product yield was 60% after 20 min (Table 2, entry 16). While for the MMCF@Thr-Pd heterogeneous catalyst under the same conditions, the product yield is up to 95% (Table 2, entry 2). According to these results, the large surface area and pores of the MMCF support facilitate the diffusion of reactants in the pores of the MMCF support to interact with the catalytic centers. On the other hand, the heterogeneous palladium complex with MMCF magnetic nanocomposite is an easy and efficient way to separate and recycle the palladium complex from the reaction mixture by an external magnetic field. Also, the model reaction was performed using MMCF@Pd nanoparticles under ligand-free and similar reaction conditions (Table 2, entry 17). In this case, the desired product yield is reduced to 45%. This result

Table 7 Catalytic Heck coupling reaction of aryl halides with alkene in the presence of MMCF@Thr-Pd

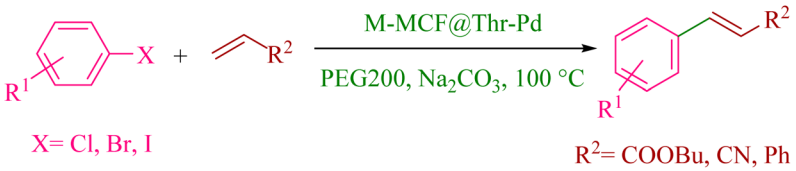

Entry	Ar–X	Alkene	Product	Time (min)	Yield (%)[a,b]	TOF (h^{-1})
1	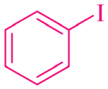	Butyl acrylate	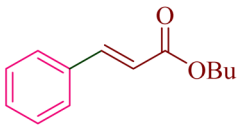	30	96	151.18
2	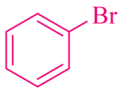	Butyl acrylate	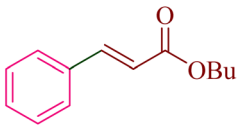	60	87	68.50
3	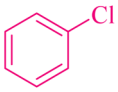	Butyl acrylate	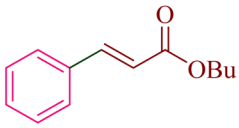	240	70	13.77
4	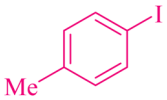	Butyl acrylate	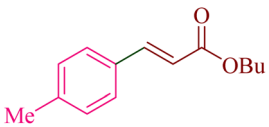	35	95	128.23
5	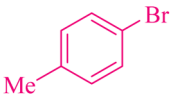	Butyl acrylate	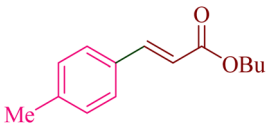	50	88	83.14
6	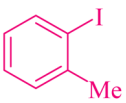	Butyl acrylate	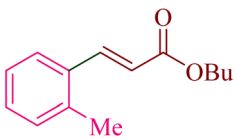	50	91	85.98
7	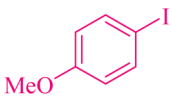	Butyl acrylate	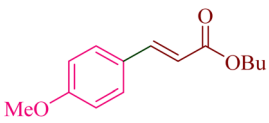	30	90	141.73
8	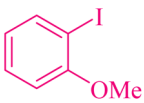	Butyl acrylate	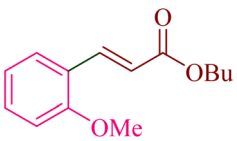	60	88	69.29
9	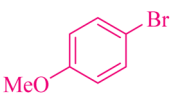	Butyl acrylate	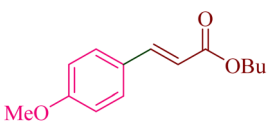	40	85	100.39
10	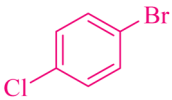	Butyl acrylate	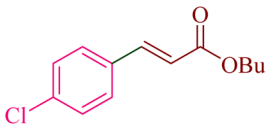	75	92	57.95

Table 7 (*Contd.*)

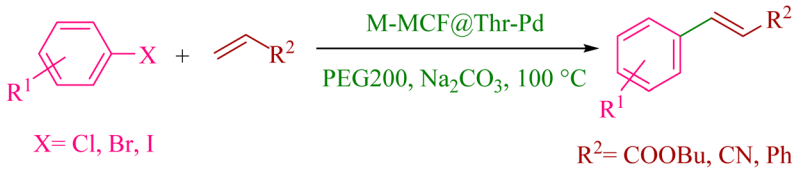

Entry	Ar–X	Alkene	Product	Time (min)	Yield (%)[a,b]	TOF (h^{-1})
11	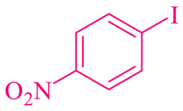	Butyl acrylate	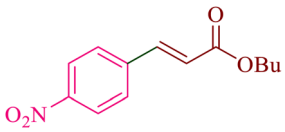	70	90	60.74
12	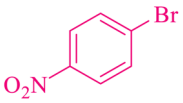	Butyl acrylate	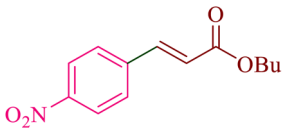	110	85	36.50
13	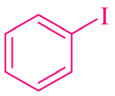	Acrylonitrile	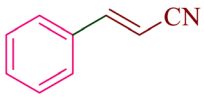	180	90	23.62
14	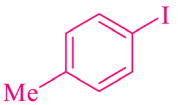	Acrylonitrile	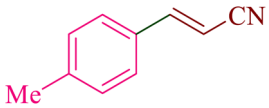	270	85	14.87
15	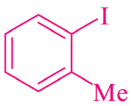	Acrylonitrile	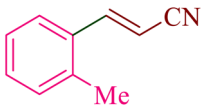	330	78	11.16
16	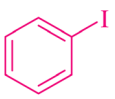	Phenyl styrene	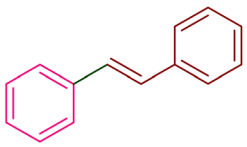	360	85	11.15
17	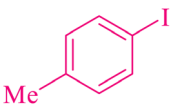	Phenyl styrene	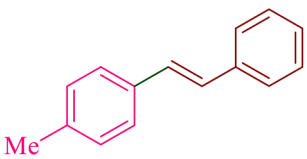	600	75	5.90
18	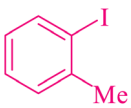	Phenyl styrene	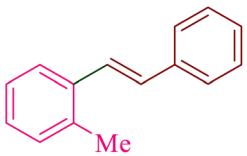	600	63	4.96

[a] Reaction conditions: aryl halides (1 mmol), alkene (1.2 mmol), Na_2CO_3 (3 mmol), M-MCF@Thr-Pd (0.0127 mmol), PEG200 (2 mL) and 100 °C. [b] Isolated yield.

shows that the catalytic activity of the nanocatalyst is reduced in the absence of a ligand. The ligand is coordinated with palladium to activate the catalytic sites.

With the optimized reactions conditions in hand (Table 2, entry 2), the substrate scope of the aryl halides and phenylboronic acid was studied in the presence of K_2CO_3 and 0.0079 mmol of MMCF@Thr-Pd in EtOH at 60 °C, and the results are summarized in Table 3. Different aryl halides containing electron-withdrawing and electron-donating groups reacted efficiently with phenylboronic acid, and excellent isolated yields and high TOF values were obtained.

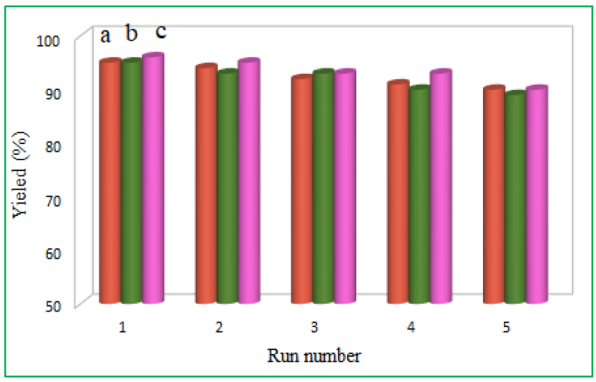

Fig. 9 Reusability of the MMCF@Thr-Pd nanocatalyst in (a) Suzuki reaction, (b) Stille reaction, and (c) Heck reaction.

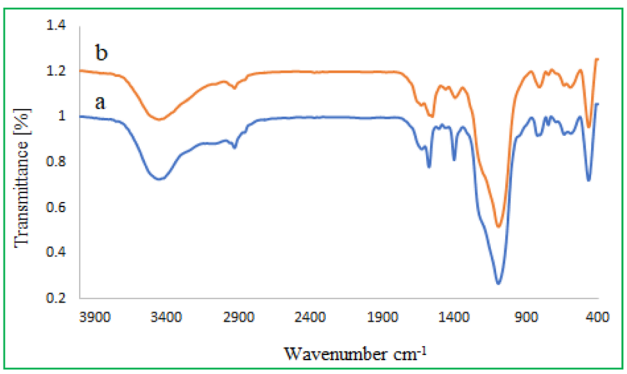

Fig. 10 FT-IR spectra of (a) MMCF@Thr-Pd and (b) recovered MMCF@Thr-Pd.

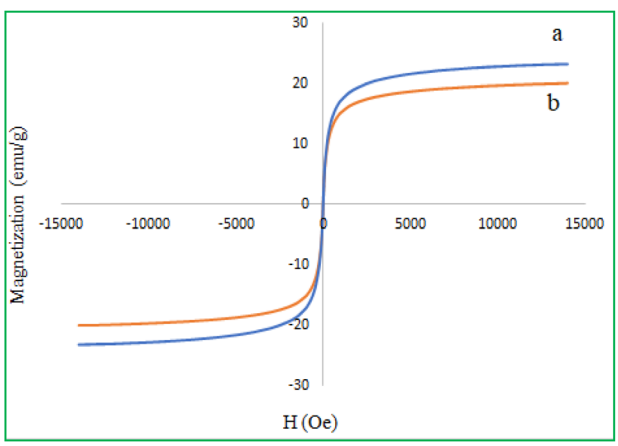

Fig. 11 Magnetization curves for (a) MMCF@Thr-Pd and (b) recovered MMCF@Thr-Pd.

Having demonstrated that the MMCF@Thr-Pd nanocatalyst was very effective for the Suzuki reaction, its activity was also examined in the Stille coupling reaction of various aryl halides with triphenyltin chloride. The reaction between iodobenzene and triphenyltin chloride was selected as a model coupling reaction. The model reaction was performed using different bases, such as K_2CO_3, Na_2CO_3, NaOH, KOH, and Et_3N, and a series of solvents, such as EtOH, H_2O, DMF, DMSO, PEG-200, and dioxane at the specific temperatures (Table 4, entries 5–13). In addition, the effect of the amount of catalyst on Stille coupling was also tested (Table 4, entries 2–4).

The optimal conditions of the Stille coupling reaction were presented in Table 4, entry 3. Based on the optimized reaction conditions, the generality of Stille coupling reactions between iodobenzene and triphenyltin chloride was examined in the presence of K_2CO_3 and 0.0079 mmol of MMCF@Thr-Pd at 80 °C in PEG-200, and the results are listed in Table 5.

According to the above satisfactory results of Suzuki and Stille reactions, the activity of MMCF@Thr-Pd nanocatalyst for Heck reaction was also evaluated. The reaction between iodobenzene and *n*-butyl acrylate was chosen as a model reaction to determine optimal reaction conditions such as solvents, nature of the base, amount of the catalyst, and temperature (Table 6). Experimental results showed that the use of Na_2CO_3 as base and PEG-200 as solvent at 100 °C for 30 min gave the best result for the Heck reaction of iodobenzene and *n*-butyl acrylate (96%, Table 6, entry 3).

Using the optimal reaction conditions (Table 6, entry 3)., the scope of this catalytic system in the Heck reaction was extended to the reaction of *n*-butyl acrylate, acrylonitrile and phenyl styrene with aryl halides having various electron-withdrawing and electron-donating substituents. As shown in Table 7, aryl iodides and activated aryl bromides reacted well and generated the desired products in good to excellent yields (65–96%) and high TOF. It should be mentioned that when chlorobenzene was used as the substrate, a good yield was obtained (70%) (Table 7, entry 3).

Reusability of the catalyst

An inherent advantage of heterogeneous catalysts over homogeneous catalysts, which is also economically feasible, is the reusability of expensive catalysts. Thus, the recyclability of this heterogeneous Pd catalyst was investigated in Suzuki, Stille, and Heck cross-coupling reactions and is shown in Fig. 9. The model reaction of iodobenzene with phenylboronic acid (Suzuki reaction), iodobenzene with triphenyltin chloride (Stille reaction), and iodobenzene with *n*-butyl acrylate (Heck reaction) was carried out under optimized reaction conditions. To reuse the catalyst in the next step, after the completion of the reaction, the palladium catalyst was separated easily using a simple magnetic magnet, washed with ethyl acetate, and dried under a vacuum. As the results showed (Fig. 9), the palladium catalyst was recycled and reused up to five times without a significant decrease in its catalytic activity.

The recovered catalyst that was used in the Suzuki reaction was identified by FT-IR spectrum (Fig. 10), VSM curve (Fig. 11) and SEM images (Fig. 12). The results showed that the recycled catalyst is similar to the fresh catalyst, which indicates the chemical stability of the MMCF@Thr-Pd nanocatalyst after recycling.

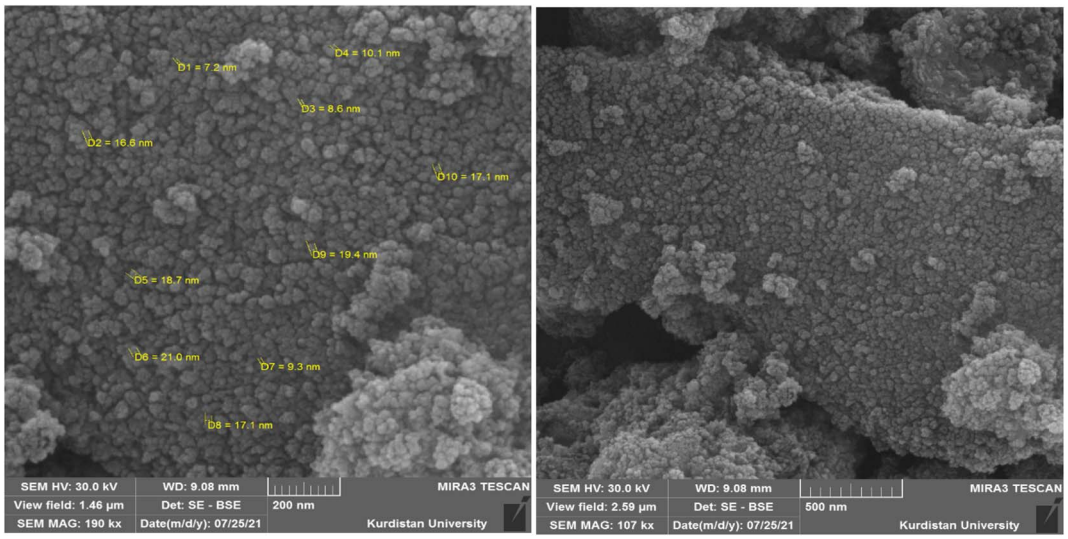

Fig. 12 SEM images of recovered MMCF@Thr-Pd.

Table 8 Comparison of MMCF@Thr-Pd with previously reported catalysts in the synthesis of 1,1′-biphenyl, and butyl cinnamate

Entry	Catalyst	Reaction condition	Time (min)	Yield[a] (%)	Ref
1	CA/Pd(0) (0.5–2.0 mol%)	Iodobenzene (1 mmol), phenylboronic acid (1 mmol), K_2CO_3 (2 mmol), water (10 mL), 100 °C	120	94	43
2	$PdCl_2$ (0.05 mol%)	Iodobenzene (2 mmol), phenylboronic acid (2.4 mmol), L5 (0.1 mol%), Cs_2CO_3 (4 mmol), DMF (3 mL)	120	95	44
3	Pd/Au NPs (4.0 mol%)	Iodobenzene (1 mmol), Ar0B(OH)2 (1.1 mmol), K_2CO_3 (2 mmol), EtOH/H_2O (25 mL), N_2 atm, 80 °C	24 h	88	45
4	PANI-Pd (0.022 mmol)	Iodobenzene (0.98 mmol), K_2CO_3 (1.96 mmol), dioxane–water (1 : 1), phenylboronic acid (1.17 mmol), 95 °C	240	91	46
5	LDH-Pd(0) (0.03 g)	Iodobenzene (1 mmol), phenylboronic acid (1.5 mmol), K_2CO_3 (3 mmol), 1,4-dioxane–water (5 : 1) = 10 mL, 80 °C	600	96	47
6	M-MCF@Thr-Pd (0.0079 mmol)	Iodobenzene (1 mmol), phenylboronic acid (1 mmol), K_2CO_3 (3 mmol), water (10 mL), 100 °C	40	95	This work
7	SiO_2@Fe_3O_4-Pd (0.0050 mmol)	Iodobenzene (0.5 mmol), *n*-butyl acrylate (0.6 mmol), K_2CO_3 (1 mmol), EtOH (2 mL), 60 °C	460	97	48
8	Pd-Py-MCM-41 (3.12 mol%)	Iodobenzene (1 mmol), *n*-butyl acrylate (1.2 mmol), K_2CO_3 (3 mmol), DMF, 120 °C	240	94	49
9	MNP@NHC-Pd (0.56 mol%)	Iodobenzene (0.2 mmol), *n*-butyl acrylate (0.2 mmol), $NaHCO_3$ (0.2 mmol), DMF (1 mL), 120 °C	22 h	86	50
10	PdAS-V (5×10^{-5} mol equiv.)	Iodobenzene (1 mmol), *n*-butyl acrylate (1.5 mmol), Et_3N (1.5 mol equiv.), toluene, 100 °C	20 h	98	51
11	M-MCF@Thr-Pd (0.0127 mmol)	Iodobenzene (1 mmol), *n*-butyl acrylate (1.2 mmol), Na_2CO_3 (3 mmol), PEG-200 (2 mL), 100 °C	30	96	This work

[a] Isolated yield.

Hot filtration study

To investigate the heterogeneous nature of MMCF@Thr-Pd nanocatalyst, the reaction of *n*-butyl acrylate with iodobenzene was carried out under optimal conditions. After half of the reaction time (15 min), the reaction stopped and only 58% of the related product was obtained. The reaction was repeated and the catalyst was removed with a magnetic magnet at half of the reaction time, and the reaction mixture was allowed to react in the absence of the catalyst for another 15 min, and the reaction yield was 65%. During this period, no increase in product yield was observed and only 7% of the reaction of *n*-butyl acrylate with iodobenzene was obtained under conditions without palladium catalyst for another 15 min.

Comparison of the catalyst

As a comparison, we investigated the catalytic activity of MMCF@Thr-Pd nanocatalyst compared to other Pd-based catalysts reported in the literature for Suzuki and Heck cross-coupling reactions. In Table 8, the results of the reaction of iodobenzene with phenylboronic (Table 8, entries 1–6) and the reaction of iodobenzene with *n*-butyl acrylate (Table 8, entries 7–11) are presented. As can be seen, the MMCF@Thr-Pd nanocatalyst showed higher reaction yields in lower reaction times compared to previously reported catalysts. Thermal stability, low cost, non-toxic, and easy magnetic separation are the other advantages of the new MMCF@Thr-Pd nanocatalyst.

Conclusion

In this work, an L-threonine amino acid-modified MMCF magnetic nanocomposite, MMCF@Thr, was successfully synthesized and used as a solid support for the immobilization of palladium nanoparticles, MMCF@Thr-Pd. The nanocatalyst was fully characterized by various instrumental techniques and the high catalytic activities of this novel magnetic nanocomposite were investigated in Suzuki, Stille, and Heck cross-coupling reactions. All products were obtained in significant yields and appropriate TOF values. The performance of the catalyst was almost completely maintained during the reuse process and was easily reused at least five times. In addition, the new magnetic catalyst has high stability and is environmentally friendly.

Experimental

MMCF preparation

Mesostructured cellular foam (MCF) silica, was prepared according to the reported procedure.[52,53] Pluronic P123 (2 g) was added to a solution of hydrochloric acid (75 mL, 1.6 M) at room temperature. The solution was stirred by magnetic stirring until completely dissolved. Then, NH_4F (23 mg) and TMB (2 g) were added to the solution. After stirring at 40 °C for 45 min, TEOS (4.4 g) was added to the mixture and the stirring continued at 40 °C for 20 h. The milky solution was transferred into an autoclave at 100 °C for 20 h. After that, the product was filtered and it was washed several times with deionized water, and dried in a vacuum at 50 °C. The solid product was calcined for 5 h at 550 °C to yield the white MCF silica.

Magnetic γ-Fe_2O_3 nanoparticles were incorporated into the pores of mesocellular silica foams through modified procedures.[42,54] For this purpose, $Fe(NO_3)_3 \cdot 9H_2O$ (1.34 g) dissolved in methanol was added to foam silica (1 g). After the mixture was dried in an oven at 85 °C, propionic acid was added at 90 °C for 3 h to form the iron propionate complex. Then, the solid product was calcined for 30 min at 300 °C to produce MMCF.

Modification MMCF with Pd(0)–threonine complex

According to the similar procedure,[40,55] the obtained MMCF (1 g) was well dispersed in deionized water (40 mL) under ultrasonication for 20 min. Afterward, L-threonine (0.39 g, 3.0 mmol) was added and stirred under reflux for 48 h under an nitrogen atmosphere. The product was then obtained by an external magnet, washed with water and ethanol, and dried at 50 °C for 12 h to give MMCF@Thr nanoparticles. Next, the MMCF@Thr (1 g) was ultrasonicated in 35 mL of ethanol, and $Pd(OAc)_2$ (0.5 g) was added to the reaction mixture under the N_2 atmosphere then refluxed for 20 h. Then 3.0 mmol (0.11 g) of $NaBH_4$ was added to the reaction mixture and further stirred for 2 h to reduce palladium(II) to palladium(0). Finally, the obtained MMCF@Thr-Pd was collected with a magnet, washed with ethanol, and dried at 50 °C.

General procedure for Suzuki reaction

Aryl halide (1.0 mmol), phenylboronic acid (1.0 mmol), MMCF@Thr-Pd nanocatalyst (5 mg, 0.0079 mmol), and K_2CO_3 (3.0 mmol) were combined in a glass flask containing 2 mL of ethanol without degassing. The mixture was magnetically stirred at 60 °C. The end of the reaction was monitored by TLC. After completion of the reaction, the MMCF@Thr-Pd nanocatalyst was separated by applying a magnetic field and extracted with water and ethyl acetate (3 × 10 mL). The combined organic layers were dried over anhydrous Na_2SO_4. The desired products were obtained in excellent yields.

General procedure for Stille reaction

To a round-bottomed flask, PEG-200 (2 mL), K_2CO_3 (3.0 mmol), aryl halide (1.0 mmol), triphenyltin chloride (0.5 mmol), and MMCF@Thr-Pd nanocatalyst (5 mg, 0.0079 mmol) were added without degassing and stirred at 80 °C. After completion of the reaction (monitored by TLC), the MMCF@Thr-Pd nanocatalyst was separated with a magnet, and the product was extracted with water and ethyl acetate (3 × 10 mL). The combined organic phases were dried and concentrated to give the corresponding products in good to excellent yields.

General procedure for Heck reaction

Alkene (1.2 mmol), aryl halide (1.0 mmol), Na_2CO_3 (3.0 mmol), the synthesized MMCF@Thr-Pd nanocatalyst (8 mg, 0.0127 mmol), and 2 mL of PEG-200 were added into a round-bottomed flask without degassing. The resulting mixture was mechanically stirred at 100 °C. TLC analysis was used to evaluate the

reaction progress. After completion, the MMCF@Thr-Pd nanocatalyst was removed by an external magnet. The resultant organic phase was washed with distilled water and extracted with ethyl acetate (3 × 10 mL). The organic phase was dried over anhydrous Na_2SO_4. The desired products were obtained in good to excellent yields.

Selected spectral data

2-Methyl-1,1′-biphenyl. Mp: oil,[56] ^{1}H NMR (300 MHz, $CDCl_3$): δ (ppm) = 7.53–7.48 (m, 2H), 7.47–7.42 (m, 3H), 7.39–7.35 (m, 4H), 2.38 (s, 3H).

4-Chloro-1,1′-biphenyl. Mp: 77–79 °C,[57] ^{1}H NMR (300 MHz, $CDCl_3$): δ (ppm) = 7.60–7.56 (m, 2H), 7.56–7.52 (m, 2H), 7.51–7.46 (m, 2H), 7.44–7.40 (m, 1H), 7.38–7.35 (m, 2H).

Butyl 3-(4-methoxyphenyl)acrylate. Mp: oil,[58] ^{1}H NMR (300 MHz, $CDCl_3$): δ (ppm) = 7.67 (d, J = 15.6 Hz, 1H), 7.51 (d, J = 8.7 Hz, 2H), 6.93 (d, J = 8.7 Hz, 2H), 6.35 (d, J = 16.0 Hz, 1H), 4.23 (t, J = 6.4 Hz, 2H), 3.86 (s, 3H), 1.74–1.68 (m, 2H), 1.52–1.43 (m, 2H), 1.01 (t, J = 7.6 Hz, 3H).

Butyl 3-(2-methylphenyl)acrylate. Mp: oil,[59] ^{1}H NMR (300 MHz, $CDCl_3$): δ (ppm) = 8.02 (d, J = 16.0 Hz, 1H), 7.60–7.58 (m, 1H), 7.31–7.30 (m, 1H), 7.26–7.20 (m, 2H), 6.40 (d, J = 16.0 Hz, 1H), 4.25 (t, J = 6.8 Hz, 2H), 2.48 (s, 3H), 1.77–1.70 (m, 2H), 1.53–1.43 (m, 2H), 1.01 (t, J = 7.2 Hz, 3H).

Conflicts of interest

There are no conflicts to declare.

Acknowledgements

We gratefully acknowledge the financial support of this research by the University of Kurdistan and Bu-Ali Sina University.

Notes and references

1 M. Busch, M. D. Wodrich and C. Corminboeuf, *ACS Catal.*, 2017, **7**, 5643–5653.
2 A. Biffis, P. Centomo, A. Del Zotto and M. Zecca, *Chem. Rev.*, 2018, **118**, 2249–2295.
3 S. M. McAfee, J. S. McCahill, C. M. Macaulay, A. D. Hendsbee and G. C. Welch, *RSC Adv.*, 2015, **5**, 26097–26106.
4 S. Kumari, S. Layek and D. D. Pathak, *New J. Chem.*, 2017, **41**, 5595–5604.
5 A. Ogata, C. Furukawa, K. Sakurai, H. Iba, Y. Kitade and Y. Ueno, *Bioorg. Med. Chem. Lett.*, 2010, **20**, 7299–7302.
6 J. M. Richardson and C. W. Jones, *J. Catal.*, 2007, **251**, 80–93.
7 S. Jagtap, *Catalysts*, 2017, **7**, 267.
8 K. Zhan, P. Lu, J. Dong and X. Hou, *Chin. Chem. Lett.*, 2020, **31**, 1630–1634.
9 L. Jin, J. Qian, N. Sun, B. Hu, Z. Shen and X. Hu, *Chem. Commun.*, 2018, **54**, 5752–5755.
10 H.-J. Ai, C.-X. Cai, X. Qi, J.-B. Peng, F. Zheng and X.-F. Wu, *Tetrahedron Lett.*, 2017, **58**, 3846–3850.
11 F. Rajabi and W. R. Thiel, *Adv. Synth. Catal.*, 2014, **356**, 1873–1877.
12 Y. Liu and X. Bai, *Appl. Organomet. Chem.*, 2017, **31**, e3561.
13 B. Zhang, Z. Ye, M. Qin, Q. Wang, Y. Du, C. Qi and L. Shao, *J. Appl. Polym. Sci.*, 2021, **138**, 49666.
14 Q. Du, W. Zhang, H. Ma, J. Zheng, B. Zhou and Y. Li, *Tetrahedron*, 2012, **68**, 3577–3584.
15 X. Chen, D. Qian, G. Xu, H. Xu, J. Dai and Y. Du, *Colloids Surf., A*, 2019, **573**, 67–72.
16 M. Lamblin, L. Nassar-Hardy, J. C. Hierso, E. Fouquet and F. X. Felpin, *Adv. Synth. Catal.*, 2010, **352**, 33–79.
17 R. Ma, P. Yang and F. Bian, *New J. Chem.*, 2018, **42**, 4748–4756.
18 B. Agrahari, S. Layek, R. Ganguly and D. D. Pathak, *Inorg. Chim. Acta*, 2018, **471**, 345–354.
19 K. R. Balinge, A. G. Khiratkar and P. R. Bhagat, *J. Organomet. Chem.*, 2018, **854**, 131–139.
20 M. Nasrollahzadeh, N. Motahharifar, F. Ghorbannezhad, N. S. S. Bidgoli, T. Baran and R. S. Varma, *Mol. Catal.*, 2020, **480**, 110645.
21 A. Ohtaka, M. Kawase, S. Aihara, Y. Miyamoto, A. Terada, K. Nakamura, G. Hamasaka, Y. Uozumi, T. Shinagawa and O. Shimomura, *ACS Omega*, 2018, **3**, 10066–10073.
22 Y. Wang, C. Lu, G. Yang, Z. Chen and J. Nie, *React. Funct. Polym.*, 2017, **110**, 38–46.
23 A. A. Ibrahim, A. Lin, M. S. Adly and M. S. El-Shall, *J. Catal.*, 2020, **385**, 194–203.
24 M. Hosseini-Sarvari, Z. Razmi and M. M. Doroodmand, *Appl. Catal., A*, 2014, **475**, 477–486.
25 C. Liu, C. Cao, J. Liu, X. Wang, Y. Zhu and W. Song, *J. Mater. Chem.*, 2017, **5**, 17464–17469.
26 R. Yu, R. Liu, J. Deng, M. Ran, N. Wang, W. Chu, Z. He, Z. Du, C. Jiang and W. Sun, *Catal. Sci. Technol.*, 2018, **8**, 1423–1434.
27 S. Molaei and M. Ghadermazi, *Microporous Mesoporous Mater.*, 2021, **319**, 110990.
28 H. A. Elazab, A. R. Siamaki, S. Moussa, B. F. Gupton and M. S. El-Shall, *Appl. Catal., A*, 2015, **491**, 58–69.
29 A. Ghorbani-Choghamarani and M. Norouzi, *Appl. Organomet. Chem.*, 2016, **30**, 140–147.
30 Q. Yue, J. Sun, Y. Kang and Y. Deng, *Angew. Chem.*, 2020, **132**, 15936–15949.
31 F. Yang, X. Hu, S. Gao, X. Liu, S. Zhou and Y. Kong, *J. Alloys Compd.*, 2020, **842**, 155817.
32 L. Wei, Y. Zhao, Y. Zhang, C. Liu, J. Hong, Q. Xiao, H. Xiong and J. Li, *ChemCatChem*, 2017, **9**, 3895–3903.
33 C. Xin, Y. Ren, Z. Zhang, L. Liu, X. Wang and J. Yang, *ACS Omega*, 2021, **6**, 7739–7745.
34 K. Grzelak, M. Ziolek and M. Trejda, *Catal. Commun.*, 2020, **142**, 106045.
35 B. Zuo, Q. Deng, H. Shao, B. Cao, Y. Fan, W. Li and M. Huang, *ACS Appl. Nano Mater.*, 2021, **4**, 1831–1840.
36 A. Jha, C. R. Patil, A. C. Garade and C. V. Rode, *Ind. Eng. Chem. Res.*, 2013, **52**, 9803–9811.
37 M. T. P. da Silva, J. Villarroel-Rocha, C. F. Toncón-Leal, F. F. Barbosa, M. O. Miranda, M. A. M. Torres, K. Sapag, S. B. Pergher and T. P. Braga, *Microporous Mesoporous Mater.*, 2021, **310**, 110582.

38 S. Zhou, C. Song, W. Kong, B. Wang and Y. Kong, *Appl. Surf. Sci.*, 2020, **527**, 146853.
39 C. Petit, Y. Kim, S.-K. Lee, J. Brown, E. Larsen, D. R. Ronning, J.-W. Suh and C.-M. Kang, *ACS Omega*, 2018, **3**, 1178–1186.
40 Z. Shirvandi, A. Rostami and A. Ghorbani-Choghamarani, *Nanoscale Adv.*, 2022, **4**, 2208–2223.
41 M. Hajjami and Z. Shirvandi, *J. Iran. Chem. Soc.*, 2020, **17**, 1059–1072.
42 D. Lee, J. Lee, H. Lee, S. Jin, T. Hyeon and B. M. Kim, *Adv. Synth. Catal.*, 2006, **348**, 41–46.
43 V. W. Faria, D. G. Oliveira, M. H. Kurz, F. F. Gonçalves, C. W. Scheeren and G. R. Rosa, *RSC Adv.*, 2014, **4**, 13446–13452.
44 S. J. Sabounchei and A. Hashemi, *Inorg. Chem. Commun.*, 2014, **47**, 123–127.
45 M. Nasrollahzadeh, A. Azarian, M. Maham and A. Ehsani, *J. Ind. Eng. Chem.*, 2015, **21**, 746–748.
46 H. A. Patel, A. L. Patel and A. V. Bedekar, *Appl. Organomet. Chem.*, 2015, **29**, 1–6.
47 S. Singha, M. Sahoo and K. Parida, *Dalton Trans.*, 2011, **40**, 7130–7132.
48 P. Li, L. Wang, L. Zhang and G. W. Wang, *Adv. Synth. Catal.*, 2012, **354**, 1307–1318.
49 M. Nikoorazm, A. Ghorbani-Choghamarani and A. Jabbari, *J. Porous Mater.*, 2016, **23**, 967–975.
50 A. Z. Wilczewska and I. Misztalewska, *Organometallics*, 2014, **33**, 5203–5208.
51 Y. M. Yamada, K. Takeda, H. Takahashi and S. Ikegami, *Tetrahedron Lett.*, 2003, **44**, 2379–2382.
52 L. Wei, Y. Zhao, Y. Zhang, C. Liu, J. Hong, H. Xiong and J. Li, *J. Catal.*, 2016, **340**, 205–218.
53 P. Schmidt-Winkel, W. W. Lukens, D. Zhao, P. Yang, B. F. Chmelka and G. D. Stucky, *J. Am. Chem. Soc.*, 1999, **121**, 254–255.
54 Z. Shokri, N. Azimi, S. Moradi and A. Rostami, *Appl. Organomet. Chem.*, 2020, **34**, e5899.
55 M. Hajjami, Z. Shirvandi and Z. Yousofvand, *J. Porous Mater.*, 2017, **24**, 1461–1472.
56 O. Diebolt, P. Braunstein, S. P. Nolan and C. S. Cazin, *Chem. Commun.*, 2008, 3190–3192.
57 M. C. Hong, M. C. Choi, Y. W. Chang, Y. Lee, J. Kim and H. Rhee, *Adv. Synth. Catal.*, 2012, **354**, 1257–1263.
58 A. Ghorbani-Choghamarani, B. Tahmasbi, R. H. Hudson and A. Heidari, *Microporous Mesoporous Mater.*, 2019, **284**, 366–377.
59 D. Liu, C. Zhang, F. Wang, Z. Huang, N. Zhang, H. Zhou and Y. Kuang, *J. Mater. Chem.*, 2015, **3**, 16583–16589.